How to cite: *Angew. Chem. Int. Ed.* **2020**, *59*, 14281 – 14285
International Edition: doi.org/10.1002/anie.202004102
German Edition: doi.org/10.1002/ange.202004102

Supramolecular Chemistry **Hot Paper**

Helical Toroids Self-Assembled from a Binary System of Polypeptide Homopolymer and its Block Copolymer

Pengfei Xu[+], Liang Gao[+], Chunhua Cai, Jiaping Lin,* Liquan Wang, and Xiaohui Tian*

Abstract: *Toroids and helices are fundamental geometrical structures in nature. Polymers can self-assemble into various nanostructures, including both toroids and helices; however, nanostructures combining toroidal and helical morphologies (that is, helical toroids) are rarely observed. A binary system is reported containing polypeptide homopolymer and its block copolymer, which can hierarchically self-assemble into uniform helical nanotoroids in solution. The formation of the helical toroids is a successive two-step process. First, the homopolymers aggregate into fibrils and convolve into toroids, thereby resembling the toroidal condensation of deoxyribonucleic acid (DNA) chains. Second, the block copolymers self-assemble on the homopolymer toroids and result in helical surface patterns. Additionally, the chirality of the surface helical patterns can be varied by the chirality of the polypeptide block copolymers.*

Nanotoroids have attracted considerable attention because of their unique geometry and properties, such as serving as nanoreactors or versatile templates for functional structures, optoelectronic properties, and potential biological applications.[1] Polymer self-assembly allows the construction of various nanostructures, including spheres, cylinders, vesicles, and disks.[2] In terms of topological structures, toroids can be viewed as ring-shaped cylinders or hollow disks. In fact, toroidal nanostructures usually originate from cylinders, vesicles, or disks with a complex morphology evolution process.[3,4] However, these routes usually suffer from ill-defined morphology and less controllable process. Therefore, it is desirable to find an efficient approach to prepare uniform toroids.

Nature has the ability to create well-defined structures of high order.[5] For example, in biological systems, DNA chains in some viruses and sperm cells, as well as some semiflexible biopolymers (for example, xanthan), are able to collapse into uniform toroids through a unique loop-and-wind process.[6] Mimicking nature is an effective and feasible approach to prepare well-defined structures. However, to the best of our knowledge, there are few reports on the formation of toroids by synthetic polymers via such a highly efficient loop-and-wind route.

In addition to toroids, helical structures are also intriguing and ubiquitous in nature;[7] for example, DNA,[8a] collagen,[8b] and tobacco mosaic virus (TMV)[8c] usually possess helical structures on different size scales. Helical structures have potential applications in diverse fields, such as chiral recognition, enantioselective catalysis, and enantioseparation.[7,9] As reported in the literature, a variety of helical nanostructures with fiber-like, tubular, and spherical morphologies can be self-assembled from various building blocks.[7,10] Considering the delicate morphologies and special functions of the toroid and the helix, their combined morphology (that is, a toroidal helical structure), could be of significant fundamental interest. However, toroidal helical structures have rarely been reported.

Herein, we report an intriguing finding of the formation of uniform nanotoroids with helical surface patterns self-assembled from poly(γ-benzyl-L-glutamate) (PBLG) homopolymers and poly(γ-benzyl-L-glutamate)-*block*-poly(ethylene glycol) (PBLG-*b*-PEG) block copolymers (BCPs) in solution. In such a unique structure, PBLG homopolymers aggregate into fibrils and then convolve into a toroid, while PBLG-*b*-PEG BCPs self-assemble into helical patterns on the toroid.

Helical nanotoroids were prepared by a selective precipitation method. First, $PBLG_{3744}$ homopolymer and $PBLG_{78}$-*b*-PEG_{45} block copolymer (the subscripts denote the degree of polymerization of each block) were dissolved in a mixed solvent of tetrahydrofuran : *N*,*N*'-dimethylformamide (THF:DMF, 3:7 by volume). The weight ratio of PBLG-*b*-PEG to PBLG was 1:1, and the initial polymer concentration was 0.2 $g\,L^{-1}$. To the polymer solution, water (a selective solvent for PEG blocks) was subsequently added under stirring, followed by dialyzing against water to remove the organic solvents (experimental details are provided in Section 1 of the Supporting Information).

As shown in Figures 1 a–c, scanning electron (SEM), transmission electron (TEM), and atomic force (AFM) microscopy observations revealed that uniform toroids with helical surface patterns were obtained. Notably, the helical patterns on the toroids exclusively possess a right-handed chirality (Figure 1 a inset), which should be related to the right-handed chirality of the PBLG segment. As estimated from the SEM images, the inner diameter (D_{inner}), outer diameter (D_{outer}), and width (d_{toroid}) of the helical toroids are approximately 154 nm, 418 nm, and 132 nm, respectively. The AFM height profile shows a height of approximately 108 nm for the toroidal nanostructures (Figure 1 c inset), which is

[*] P. Xu,[+] Dr. L. Gao,[+] Prof. Dr. C. Cai, Prof. Dr. J. Lin, Dr. L. Wang, Prof. Dr. X. Tian
Shanghai Key Laboratory of Advanced Polymeric Materials
Key Laboratory for Ultrafine Materials of Ministry of Education
School of Materials Science and Engineering
East China University of Science and Technology
Shanghai 200237 (China)
E-mail: caichunhua@ecust.edu.cn
jlin@ecust.edu.cn

[+] These authors contributed equally to this work.

Supporting information and the ORCID identification number(s) for the author(s) of this article can be found under: https://doi.org/10.1002/anie.202004102.

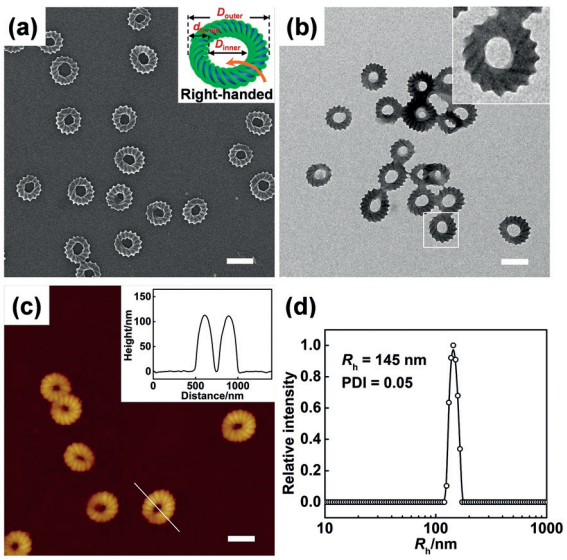

Figure 1. Helical nanotoroids self-assembled from the polymer mixtures. a) SEM image; inset is a scheme of helical nanotoroids. b) TEM image; inset presents a representative magnified image. c) AFM image of helical toroids self-assembled from the $PBLG_{78}$-*b*-PEG_{45}/$PBLG_{3744}$ mixture; inset presents the AFM height profile along the white line. d) Apparent hydrodynamic radius (R_h) distribution of the helical toroids in water (scattering angle of 90°). The weight fraction of BCPs in the polymer mixtures ($f_{PBLG\text{-}b\text{-}PEG}$) was 0.5. Scale bars: 400 nm.

close to the width of the helical toroids. Dynamic light scattering (DLS) testing revealed that these nanostructures have an apparent hydrodynamic radius (R_h) of approximately 145 nm (Figure 1 d), and the R_h distribution is very narrow (polydispersity index (PDI) = 0.05), which indicates high unity in the size of these helical toroids.

To get insights into the role of both the BCPs and homopolymers in such assemblies, we examined the effect of the weight fraction of PBLG-*b*-PEG in polymer mixtures ($f_{PBLG\text{-}b\text{-}PEG}$) on the self-assembled morphologies. Without the homopolymers (that is, $f_{PBLG\text{-}b\text{-}PEG} = 1$), spherical structures are observed for the PBLG-*b*-PEG BCPs (Supporting Information, Figure S2). It should be noted that, apart from spherical aggregates, PBLG-*b*-PEG BCPs can self-assemble into aggregates with other morphologies (for example, needle-like, worm-like, and disk-like assemblies), depending on the molecular weight, assembly conditions, and methods.[11] When homo-PBLG is added, helical toroidal structures are formed. As shown in Figures 2 a–c, as $f_{PBLG\text{-}b\text{-}PEG}$ decreases from 0.8 to 0.2 the helical nanostructures on the toroids become less visible. Furthermore, in the absence of PBLG-*b*-PEG BCPs (that is, $f_{PBLG\text{-}b\text{-}PEG} = 0$), the PBLG homopolymers self-assemble into plain toroids (Figure 2 d). The stability experiment revealed that the helical toroids are stable in solution (Supporting Information, Figure S3). The dependence of morphology on the $f_{PBLG\text{-}b\text{-}PEG}$ suggests that the PBLG homopolymers form toroids and they can serve as templates for the assembly of PBLG-*b*-PEG BCPs.

To verify this proposition, we designed a two-step assembly experiment (Figure 2 e). In the first step, the $PBLG_{78}$-*b*-PEG_{45} BCPs and $PBLG_{3744}$ homopolymers were separately dissolved in THF/DMF (3/7 by volume), and then 10.0 vol% of water was added to these solutions. In this situation, the PBLG homopolymers self-assemble into plain toroids (Figure 2 f), while the PBLG-*b*-PEG BCPs still dissolve in solution since the water content is lower than the critical water content (CWC; the CWC values of homo-PBLG and PBLG-*b*-PEG are 4.7 and 10.9 vol%, respectively; Supporting Information, Figure S4). In the second step, the two polymer solutions were mixed, followed by adding more water and dialyzing against water. As shown in the inset of Figure 2 f, helical toroids are observed which are similar to those obtained via the direct coassembly approach. Moreover, as the added water content in the first step increases (higher than the CWC value of PBLG-*b*-PEG), the helical nanostructures on the toroid surfaces become less visible and small aggregates formed by PBLG-*b*-PEG were observed (Supporting Information, Figure S5). Through such a two-step self-assembly experiment, the proposed mechanism is further confirmed; that is, the formation of helical toroids is a hierarchical self-assembly process that involves

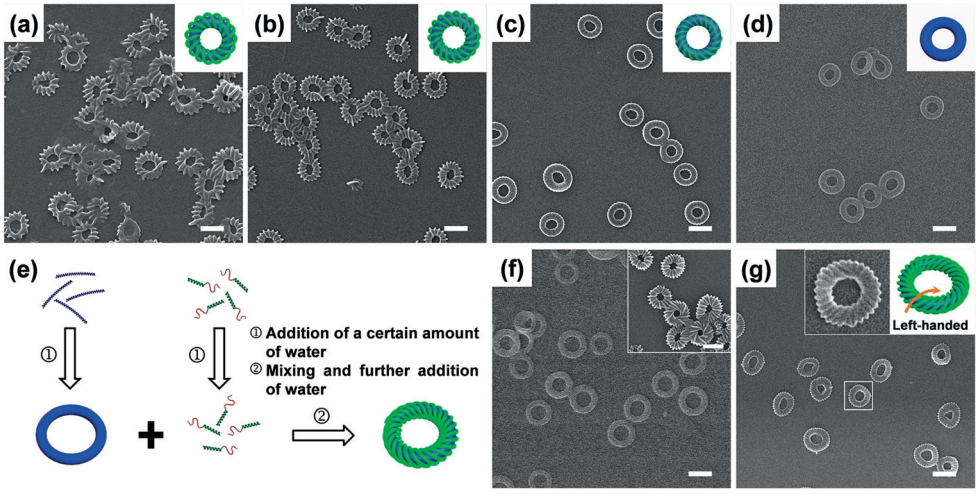

Figure 2. Structure of the helical nanotoroids. a–d) SEM images of aggregates self-assembled from PBLG-*b*-PEG/PBLG with various $f_{PBLG\text{-}b\text{-}PEG}$ values: a) 0.8, b) 0.6, c) 0.2, and d) 0; insets show schemes of the aggregates. e) Representation for the fabrication of helical toroids through a two-step self-assembly approach. f) SEM image of plain toroids assembled from PBLG homopolymers at a water content of 10.0 vol% in the first step; inset shows an SEM image of helical toroids assembled from PBLG-*b*-PEG/PBLG mixtures through a two-step self-assembly experiment. g) SEM image of helical toroids self-assembled from the $PBDG_{82}$-*b*-PEG_{45}/$PBLG_{3744}$ mixture; insets show a representative magnified image and a schematic of the helical nanotoroids. Scale bars: 400 nm.

the formation of toroids and the formation of helical patterns on the toroid surfaces.

Considering the fact that the BCPs assemble on the toroidal template of homopolymers, the molecular characteristics of the BCPs should be pivotal for the morphology of surface patterns. The effect of the molecular weight of PBLG-*b*-PEG was examined. It revealed that PBLG-*b*-PEG with short PBLG length forms rough surfaces on the toroids, while for PBLG-*b*-PEG with long PBLG length, the surface patterns on the toroids adopt fewer helical features (Supporting Information, Figure S6). We also replaced PBLG blocks with poly(γ-benzyl-D-glutamate) (PBDG, which has opposite chirality to PBLG) to examine the influence of the chirality of polypeptide blocks. Under similar preparation conditions, the PBDG-*b*-PEG/PBLG mixture self-assembled into helical toroids with left-handed helical surface patterns that have the opposite chirality to those formed from the PBLG-*b*-PEG/PBLG mixture (Figure 2g). When a mixture of PBDG-*b*-PEG and PBLG-*b*-PEG was used to co-assemble with PBLG homopolymers (the weight ratio PBLG-*b*-PEG/PBDG-*b*-PEG/PBLG = 1/1/2), toroidal structures with achiral surface patterns were observed (Supporting Information, Figure S7). Additionally, the chirality of the polypeptide homopolymers exerts less effect on the chirality of the surface nanostructures (Supporting Information, Figure S7). These results suggest that the chirality of polypeptide blocks is an important parameter determining the chirality of the assembled nanostructures.

As revealed from the preceding results, the toroidal template of homo-PBLG is fundamental for the formation of a helical toroid. In the following content, we examined the formation mechanism of homo-PBLG toroids by monitoring the morphology evolution of the homo-PBLG assemblies under various water additions. As shown in Figure 3a, when 4.7 vol% of water was added, slender fibrils were formed. The diameter of the fibrils is estimated to be approximately 25 nm and the length is up to several micrometers. When the water content was increased to 4.9 vol%, a racquet structure possessing a loop at one end of the fibril was observed (Figure 3b). This unique structure is considered an intermediate state for the formation of toroids. Upon further increasing the water content, toroidal structures appeared (Figure 3c). When the water content reached 6.0 vol%, toroids with uniform size were produced exclusively (Figure 3d). Such morphology transitions are also confirmed by TEM results (Supporting Information, Figure S8). Notably, the length of the initial fibrils is much longer than the circumference of the formed toroids, while the diameter of the loop along the racquet structures (approximately 330 nm) is close to the inner diameter of the toroids (approximately 320 nm). Therefore, it can be deduced that the toroids are formed by convolving the fibrils around the loop of the racquet structure.

To monitor the self-assembly process of homopolymer toroids in situ, we measured the R_h values of the assemblies in solution at various added water contents (Figure 3e). The mean R_h of PBLG homopolymers in the original organic solvent is approximately 23.7 nm (the water content is 0 vol%), suggesting that homo-PBLG are mainly in the

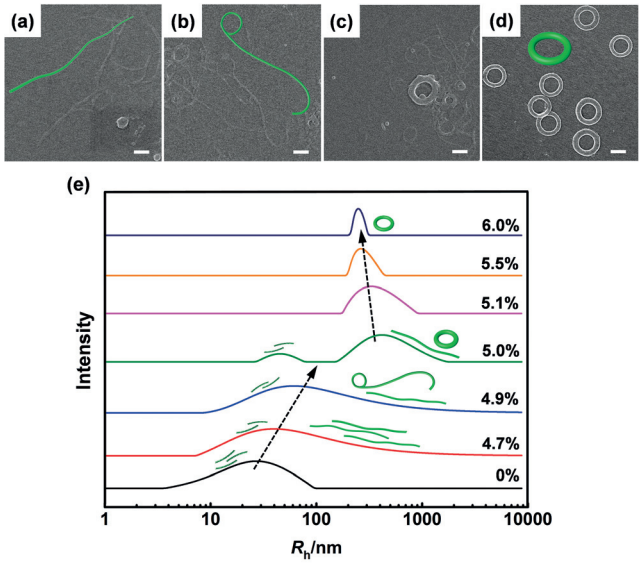

Figure 3. Formation process of the homo-PBLG toroids. a–d) SEM images of the aggregates self-assembled from $PBLG_{3744}$ homopolymers at various water contents: a) 4.7 vol%, b) 4.9 vol%, c) 5.0 vol%, and d) 6.0 vol%; insets show schemes of the corresponding aggregates. Scale bars: 300 nm. e) Plots of the R_h distribution of aggregates assembled from $PBLG_{3744}$ homopolymers vs. water content.

unimer form.[12a,13b] The broad distribution of the peak could result from some association of the PBLG chains in solution because of the π–π interactions of the side phenyl groups.[12] With the addition of water, the peak maximum of R_h shifted toward higher values, and the R_h distribution broadened, indicating the formation of homopolymer fibrils. At a water content of 5.0 vol%, a double peak distribution (that is, 46.1 nm and 390.2 nm) of R_h was observed. The peak with a higher R_h value corresponds to the aggregates (that is, the initial toroidal aggregates and fibrous aggregates shown in Figure 3c), while the peak with a lower R_h value corresponds to the homo-PBLG molecules. Upon increasing the water content to 5.1 vol%, the peak attributed to the homo-PBLG molecules disappeared, suggesting that most homo-PBLG molecules form fibrils. Upon further increasing the water content, the R_h distribution gradually narrowed, which indicates that the fibrous aggregates gradually convolute into toroids (Figure 3d). These DLS results for the in situ toroidal formation process are in good agreement with the SEM observations.

It is well known that when water is added to the homo-PBLG solution, the driving force for aggregation of the PBLG gradually increases because of hydrophobic interactions. Subsequently, the homo-PBLG aggregate into fibril-like structures several microns in length (Figure 3a). As the added water content increases, a part of the slender fibril prefers to curve into a loop (Figure 3b), which is attributed to the change in the interfacial energy between the fibrous aggregates and the solvent. It is known that the formation of closed loops is a free-energy-favorable process for fiber-like structures in a selective solvent.[3a–e,k] Because of the longer length of the fibrils, it is difficult to form a closed toroid. Instead, a partly closed loop of the fibril (for example, racquet structure) is formed to reduce the free energy. The remaining

parts of the fibrils wind around the loop to form a toroid. This process resembles the toroidal convolution of DNA chains.[6b] As a result, toroids of uniform size are obtained (Figure 3d). Indeed, we found using circular dichroism (CD) spectroscopy that the interfacial energy between the fibrous aggregates and solvent is increased with the addition of water (Supporting Information, Figure S9). To lower the free energy of the system, the fibrils wind up to form toroids.

In addition, the appropriate rigidity of chains is also an important factor in affecting the toroidal morphology. It was reported that polypeptide chains with an α-helical conformation possess integral rigidity at lower molecular weights but exhibit semiflexibility at higher molecular weights.[13] In a separate experiment, when the $PBLG_{3744}$ was replaced by $PBLG_{776}$ with relatively rigid PBLG backbones, spindle-like structures rather than toroids were obtained (Supporting Information, Figure S10), suggesting that the semiflexibility of homo-PBLG owing to its high molecular weight is crucial for the formation of polypeptide toroids. We have also examined the effect of initial solvent compositions on the self-assembled structures from the PBLG-*b*-PEG/PBLG system. It was found that toroidal structures can also be formed, while the size of the toroid and surface nanostructures vary with the initial solvent composition (Supporting Information, Figure S11).

To gain a deep understanding of the formation mechanism of toroids, we performed Brownian dynamics (BD) simulations on the self-assembly behaviors. Shown in Figure 4a is the coarse-grained model of the homopolymer comprising a rigid backbone (**R** beads) and multiple pendant groups (**P** beads). The homopolymer $PBLG_{3744}$ used in the experiments was modeled as $\mathbf{R}_{50}$ (the subscript is the number of **R** beads). A **P** bead was jointed to each **R** bead to represent the pendant group of the PBLG backbone. The backbone rigidity was realized by maintaining the angle between two neighboring backbone bonds unchanged. The attractive potential was set for **R-R** and **P-P** pairwise interactions to describe the hydrophobic nature of PBLG backbones and the π–π interaction between phenyl groups, respectively.[3k,14a] The repulsive potential was given for the **R-P** interaction.[14b–d] Their interaction strengths were determined by the parameters ε_{RR}, ε_{PP}, and ε_{RP} (simulation details are given in Section 2 of the Supporting Information). In the experiments, the addition of selective solvent (water) leads to the enhancement of hydrophobicity and the aggregation of homopolymers. To simulate this situation, the interaction parameters were set as follows: $\varepsilon_{RR} = \varepsilon_{PP} = 5.0\varepsilon$ and $\varepsilon_{RP} = 1.0\varepsilon$; where ε is the energy unit in the simulation. Toroidal structures are formed under this condition (Figure 4b). In the toroidal structures, the semiflexible backbones are bent. The cross-sectional view revealed that the bent backbones are almost parallel to the arc of the toroidal structure (Figure 4c).

The formation process of toroids was examined by tracing the simulation morphologies. As shown in Figure 4d, at the initial stage ($\varepsilon_{RR} = \varepsilon_{PP} = 5.0\varepsilon$), $\mathbf{R}_{50}$ homopolymers with a length of 75σ (σ is the length unit) were randomly dispersed in the simulation box. Under this condition, with increasing simulation time, fibrous aggregates with a length of 342σ were observed. An initial loop formed by curving one end of the fibrous aggregate with time. Finally, the remaining fibrous part wound around the initial loop, resulting in the formation of a toroidal structure with a diameter of 39σ. These simulation results correlate well with the experimental observations through the comparison of the size of polymers, fibrils, and toroids from experiments and simulations (details are presented in Section 2.3 of the Supporting Information).

Note that the lengths of initial fibrous aggregates are generally polydisperse, while the final toroidal structures show low dispersity of diameter (see the SEM images and DLS results in Figure 3). Such an interesting phenomenon was also observed in the simulations. We found that the diameter of the formed toroids is determined by the interaction parameter ε_{PP} and the backbone rigidity, while it is less dependent on the length and polydispersity of the initial fibrous aggregates (Supporting Information, Figure S13). For all the fibrous aggregates in the solution, the diameter of the formed toroids is uniform, since both the interaction strength between the rods and the rigidity of homopolymers remain almost constant in the experiment.

As revealed by the experiments, the formation of helical toroids contains two stages: the formation of toroidal templates followed by the formation of helical patterns on the template surfaces. After reaching a theoretical understanding of the formation of the toroidal template, we simulated the formation of helical patterns on the toroid (Supporting Information, Figures S14 and S15). In the system containing a toroidal template and the randomly dispersed rod–coil BCP $\mathbf{R}_3\mathbf{C}_2$ (**C** represents the coil PEG blocks), increasing simulation time resulted in the adsorption of the $\mathbf{R}_3\mathbf{C}_2$ on the toroids to form a smooth surface, followed by gradual phase separation, resulting in a helical pattern on the toroidal template (Supporting Information, Figure S15). The simulation results qualitatively reproduce the formation process of helical nanostructures.

The formation process of the polypeptide toroidal template observed in the present system shows some similarities with the toroidal condensation of biopolymers such as

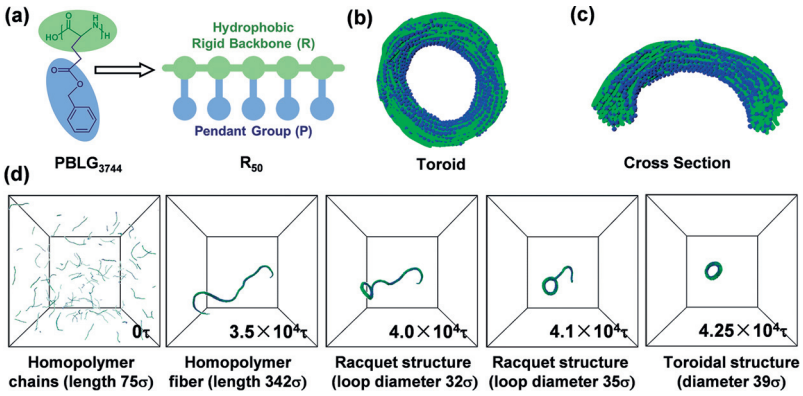

Figure 4. BD simulations for the formation of toroids. a) Coarse-grained model of $PBLG_{3744}$ in the simulation, denoted as $\mathbf{R}_{50}$. b) Top-view and c) cross-sectional view of the typical toroids obtained at $\varepsilon_{RR} = \varepsilon_{PP} = 5.0\varepsilon$. d) Simulation snapshots for the formation process of the homopolymer toroid at various simulation times.

DNA. Both toroids are produced by winding the remaining parts around the initial loop, and their dimension is determined by the initial loop size, which is related to polymer semiflexibility and self-attraction interactions and is less dependent on the polydispersity of the winding objects.[6b,14e] Such a loop-and-wind process can realize the uniformity of toroids. The present work provides a good model for deeply understanding biological phenomena.

In conclusion, uniform nanotoroids with helical surface patterns were self-assembled from a binary system containing PBLG-*b*-PEG BCPs and PBLG homopolymers. It was discovered that the PBLG homopolymers formed toroidal templates on which the PBLG-*b*-PEG BCPs self-assembled into helical patterns. The toroidal templates originated from the convolution of fibrous structures formed by PBLG homopolymers, which resembles the toroidal condensation of DNA chains. The formation of helical toroids exhibits a hierarchical characteristic. Additionally, the chirality of the surface helical patterns can be manipulated by the chirality of the polypeptide BCPs. This work enhances our ability to design polypeptide hierarchical assemblies and has potential biological applications.

Acknowledgements

This work was supported by the National Natural Science Foundation of China (51833003, 51621002, 21975073, and 51573049).

Conflict of interest

The authors declare no conflict of interest.

Keywords: helices · hierarchical assembly · polypeptides · theoretical simulation · toroids

[1] a) Y. Kim, W. Li, S. Shin, M. Lee, *Acc. Chem. Res.* **2013**, *46*, 2888 – 2897; b) A. Steinhaus, R. Chakroun, M. Müllner, T.-L. Nghiem, M. Hildebrandt, A. H. Gröschel, *ACS Nano* **2019**, *13*, 6269 – 6278; c) Z. Geng, B. Xiong, L. Wang, K. Wang, M. Ren, L. Zhang, J. Zhu, Z. Yang, *Nat. Commun.* **2019**, *10*, 4090; d) R. Djalali, J. Samson, H. Matsui, *J. Am. Chem. Soc.* **2004**, *126*, 7935 – 7939; e) M. J. Urban, P. K. Dutta, P. Wang, X. Duan, X. Shen, B. Ding, Y. Ke, N. Liu, *J. Am. Chem. Soc.* **2016**, *138*, 5495 – 5498; f) V. M. Suresh, S. J. George, T. K. Maji, *Adv. Funct. Mater.* **2013**, *23*, 5585 – 5590; g) L. Alexander, K. Dhaliwal, J. Simpson, M. Bradley, *Chem. Commun.* **2008**, 3507 – 3509.

[2] a) Y. Mai, A. Eisenberg, *Chem. Soc. Rev.* **2012**, *41*, 5969 – 5985; b) C. Cai, J. Lin, Y. Lu, Q. Zhang, L. Wang, *Chem. Soc. Rev.* **2016**, *45*, 5985 – 6012; c) R. C. Hayward, D. J. Pochan, *Macromolecules* **2010**, *43*, 3577 – 3584; d) C. Chen, R. A. L. Wylie, D. Klinger, L. A. Connal, *Chem. Mater.* **2017**, *29*, 1918 – 1945; e) S. J. Holder, N. A. J. M. Sommerdijk, *Polym. Chem.* **2011**, *2*, 1018 – 1028.

[3] a) D. J. Pochan, Z. Chen, H. Cui, K. Hales, K. Qi, K. L. Wooley, *Science* **2004**, *306*, 94 – 97; b) H. Cui, Z. Chen, K. L. Wooley, D. J. Pochan, *Soft Matter* **2009**, *5*, 1269 – 1278; c) X. Li, M. Deng, Y. Liu, H. Liang, *J. Phys. Chem. B* **2008**, *112*, 14762 – 14765; d) Z. Wang, W. Jiang, *Soft Matter* **2010**, *6*, 3743 – 3746; e) H. Yu, W. Jiang, *Macromolecules* **2009**, *42*, 3399 – 3404; f) M. He, L. Zhao, J. Wang, W. Han, Y. Yang, F. Qiu, Z. Lin, *ACS Nano* **2010**, *4*, 3241 – 3247; g) C. Liu, G. Chen, H. Sun, J. Xu, Y. Feng, Z. Zhang, T. Wu, H. Chen, *Small* **2011**, *7*, 2721 – 2726; h) C. Luo, Y. Liu, Z. Li, *Soft Matter* **2012**, *8*, 2618 – 2626; i) X. Li, Y. Gao, X. Xing, G. Liu, *Macromolecules* **2013**, *46*, 7436 – 7442; j) L. Chen, T. Jiang, J. Lin, C. Cai, *Langmuir* **2013**, *29*, 8417 – 8426; k) C. Yang, L. Gao, J. Lin, L. Wang, C. Cai, Y. Wei, Z. Li, *Angew. Chem. Int. Ed.* **2017**, *56*, 5546 – 5550; *Angew. Chem.* **2017**, *129*, 5638 – 5642.

[4] a) X. He, F. Schmid, *Phys. Rev. Lett.* **2008**, *100*, 137802; b) H. Huang, B. Chung, J. Jung, H. W. Park, T. Chang, *Angew. Chem. Int. Ed.* **2009**, *48*, 4594 – 4597; *Angew. Chem.* **2009**, *121*, 4664 – 4667; c) K.-J. Peng, Y.-L. Liu, *Macromolecules* **2011**, *44*, 5006 – 5012; d) X. Hong, S. Liu, Y. Wang, *Soft Matter* **2013**, *9*, 5642 – 5648; e) D. Presa-Soto, G. A. Carriedo, R. de la Campa, A. Presa Soto, *Angew. Chem. Int. Ed.* **2016**, *55*, 10102 – 10107; *Angew. Chem.* **2016**, *128*, 10256 – 10261; f) H. Qiu, A. M. Oliver, J. Gwyther, J. Cai, R. L. Harniman, D. W. Hayward, I. Manners, *Macromolecules* **2019**, *52*, 113 – 120.

[5] S. E. Naleway, M. M. Porter, J. McKittrick, M. A. Meyers, *Adv. Mater.* **2015**, *27*, 5455 – 5476.

[6] a) V. A. Bloomfield, *Biopolymers* **1997**, *44*, 269 – 282; b) N. V. Hud, I. D. Vilfan, *Annu. Rev. Biophys. Biomol. Struct.* **2005**, *34*, 295 – 318; c) G. Maurstad, B. T. Stokke, *Curr. Opin. Colloid Interface Sci.* **2005**, *10*, 16 – 21.

[7] a) M. Liu, L. Zhang, T. Wang, *Chem. Rev.* **2015**, *115*, 7304 – 7397; b) E. Yashima, N. Ousaka, D. Taura, K. Shimomura, T. Ikai, K. Maeda, *Chem. Rev.* **2016**, *116*, 13752 – 13990.

[8] a) J. D. Watson, G. S. Stent, *The Double Helix: A Personal Account of the Discovery of the Structure of DNA*, Atheneum, New York, **1980**; b) B. Brodsky, J. A. M. Ramshaw, *Matrix Biol.* **1997**, *15*, 545 – 554; c) A. Klug, *Philos. Trans. R. Soc. London Ser. B* **1999**, *354*, 531 – 535.

[9] a) T. Tu, W. Fang, X. Bao, X. Li, K. H. Dötz, *Angew. Chem. Int. Ed.* **2011**, *50*, 6601 – 6605; *Angew. Chem.* **2011**, *123*, 6731 – 6735; b) Q. Jin, L. Zhang, H. Ca, T. Wang, X. Zhu, J. Jian, M. Liu, *Langmuir* **2011**, *27*, 13847 – 13853; c) L. Zhang, T. Wang, Z. Shen, M. Liu, *Adv. Mater.* **2016**, *28*, 1044 – 1059.

[10] a) C. Cai, Y. Li, J. Lin, L. Wang, S. Lin, X.-S. Wang, T. Jiang, *Angew. Chem. Int. Ed.* **2013**, *52*, 7732 – 7736; *Angew. Chem.* **2013**, *125*, 7886 – 7890; b) Y. Yang, J. Zhang, W. Zou, S. Wu, F. Wu, A. Xie, Z. Wei, *Macromol. Rapid Commun.* **2018**, *39*, 1700591; c) S. Sun, Y. Yang, D. Li, J. Zhu, *J. Am. Chem. Soc.* **2019**, *141*, 19524 – 19528; d) C. D. Vacogne, C. Wei, K. Tauer, H. Schlaad, *J. Am. Chem. Soc.* **2018**, *140*, 11387 – 11394.

[11] a) C. Grazon, P. Salas-Ambrosio, E. Ibarboure, A. Buol, E. Garanger, M. W. Grinstaff, S. Lecommandoux, C. Bonduelle, *Angew. Chem. Int. Ed.* **2020**, *59*, 622 – 626; *Angew. Chem.* **2020**, *132*, 632 – 636; b) X. Lin, X. He, C. Hu, Y. Chen, Y. Mai, S. Lin, *Polym. Chem.* **2016**, *7*, 2815 – 2820.

[12] a) J. Helfrich, R. Hentschke, *Macromolecules* **1995**, *28*, 3831 – 3841; b) P. Doty, J. H. Bradbury, A. M. Holtzer, *J. Am. Chem. Soc.* **1956**, *78*, 947 – 954.

[13] a) S. Itou, N. Nishioka, T. Norisuye, A. Teramoto, *Macromolecules* **1981**, *14*, 904 – 909; b) M. Schmidt, *Macromolecules* **1984**, *17*, 553 – 560.

[14] a) S. Lin, N. Numasawa, T. Nose, J. Lin, *Macromolecules* **2007**, *40*, 1684 – 1692; b) L. Gao, J. Lin, L. Zhang, L. Wang, *Nano Lett.* **2019**, *19*, 2032 – 2036; c) M. A. Horsch, Z. Zhang, S. C. Glotzer, *Phys. Rev. Lett.* **2005**, *95*, 056105; d) G. K. Bourov, A. Bhattacharya, *J. Chem. Phys.* **2005**, *122*, 044702; e) L. Gao, R. Hu, P. Xu, J. Lin, L. Zhang, L. Wang, *Nanoscale* **2020**, *12*, 296 – 305.

Manuscript received: March 20, 2020
Revised manuscript received: May 5, 2020
Accepted manuscript online: May 19, 2020
Version of record online: July 1, 2020

